X-ray scattering applied to the analysis of carbon nanotubes, polymers and nanocomposites

Dispersión de rayos X aplicado al análisis de nanotubos de carbono, polímeros y nanocompuestos

M. C. García-Gutiérrez, A. Nogales, J. J. Hernández, D. R. Rueda, T. A. Ezquerra (*)

Instituto de Estructura de la Materia, CSIC, Serrano 121, 28006 Madrid, Spain

* Email de contacto: imte155@iem.cfmac.csic.es

RESUMEN:

En este trabajo de revisión mostramos que las técnicas de dispersión de rayos X a alto y bajo ángulo (WAXS y SAXS respectivamente) pueden ser una herramienta muy valiosa para caracterizar la estructura de nanotubos de carbono (CNT) y nanocompuestos CNT-polímero, en diferentes escalas de longitud. La dispersión de rayos X puede ofrecer información estructural en el rango desde nanotubos de carbono aislados, hasta agregados de CNT. Dicha información puede ser crucial de cara a diseñar materiales basados en nanotubos de carbono.

Palabras clave: Dispersión de Rayos X, WAXS, SAXS, Nanotubos de Carbono, Nanocompuestos Poliméricos.

ABSTRACT:

In this review we will show that wide and small angle X-ray scattering techniques (WAXS and SAXS respectively) can be a valuable tool to characterize the structure of carbon nanotubes (CNT) and related CNT-polymer nanocomposites at different characteristic length scales. Ranging from single carbon nanotubes to aggregates of CNTs X-ray scattering may offer structural information which can be crucial in order to design new materials based on carbon nanotubes.

Keywords: X-ray Scattering, WAXS, SAXS, Carbon Nanotubes, Polymer Nanocomposites.

REFERENCIAS Y ENLACES

[1] S. IIjima, "Helical microtubules of graphitic carbon", *Nature* **354**, 56-58 (1991).

[2] M. M. J. Treacy, T. W. Ebbesen, J. M. Gibson, "Exceptionally high Young's modulus observed for individual carbon nanotubes", *Nature* **381**, 678-680 (1996).

[3] O. Lourie, D. M. Cox, H. D. Wagner, "Buckling and collapse of embedded carbon nanotubes", *Phys. Rev. Lett*. **81**, 1638-1641 (1998)

[4] R.A. Vaia, and H.D. Wagner, "Framework for nanocomposites", *Mater. Today* **7**, 32-37 (2004).

[5] M. Terrones, "Science and technology of the twenty-first century: Synthesis, properties, and applications of carbon nanotubes" *Annu. Rev. Mater. Res.* **33**, 419-501 (2003).

[6] J. K. W. Sandler, J. E. Kirk, I. A. Kinloch, M. S. P. Shaffer, A. H. Windle, "Ultra-low electrical percolation threshold in carbon-nanotube-epoxy composites", *Polymer* **44**, 5893-5899 (2003).

[7] G. Gorriasi, M. Tortora, V. Vittoria, E. Pollet, B. Lepoittevin, M. Alexandre, P. Dubois "Vapor barrier properties of polycaprolactone montmorillonite nanocomposites: effect of clay dispersion", *Polymer* **44**, 2271-2279 (2003).

[8] R. A. Vaia, "New polymer electrolyte nanocomposites: Melt intercalation of poly(ethylene oxide) in mica-type silicates", *Adv. Mater*. **7**, 154-156 (1995).

[9] C. Domingo, "Espectroscopía Raman de nanotubos de carbono", *Opt. Pura Apl*. **40**, 175-186 (2007).

[10] M. S. Dresselhaus, P. C. Eklund, "Phonons in carbon nanotubes", *Adv. Phys*. **49**, 705-814 (2000).

[11] A. Thess, R. Jee, P. Nikolaev, H. Dai, P. Petit, J. Robert, C. Xu, Y. Hee Lee, S. Gon Kim, A. G. Rinzler, D. T. Colbert, G. E. Scuseria, D. Tomanek, J. E. Fischer, R. E. Smalley, "Crystalline ropes of metallic carbon nanotubes", *Science* **273**, 483-487 (1996).

[12] S. Rols, R. Almairac, L. Henrard, E. Anglaret, J.-L. Sauvajol, "Diameter distribution of single wall carbon nanotubes in nanobundles"; *Eur. Phys. J. B* **18**, 201-205 (2000).

[13] S. Rols, I. N. Goncharenko, R. Almairac, J. L. Sauvajol, I. Mirebeau, "Polygonization of single-wall carbon nanotube bundles under high pressure", *Phys. Rev. B* **64**, 153401 (2001).

[14] A. Oberlin, M. Endo, T. Koyama, "Filamentous growth of carbon through benzene decomposition", *J. Cryst. Growth* **32**, 335-349 (1976).

[15] E. T. Thostenson, Z. Ren, T. W. Chou, "Advances in the science and technology of carbon nanotubes and their composites: A review", *Compos. Sci. Technol.* **61**, 1899-1912 (2001).

[16] P. Nikolaev, M. J. Bronikowski, R. K. Bradley, F. Fohmud, D. T. Colbert, K. A.Smith, "Gas-phase catalytic growth of single-walled carbon nanotubes from carbon monoxide", *Chem. Phys. Lett.* **313**, 91-97 (1999).

[17] Y. L. Li, I. A. Kinloch, A. H. Windle, "Direct spinning of carbon nanotube fibers from chemical vapor deposition synthesis", *Science* **304**, 276-278 (2004).

[18] B. D. Cullity, *Elements of X-Ray Diffraction*, Addison-Wesley, Cop., Massachusetts (1978).

[19] C. Kittel, *Introduction to Solid State Physics*, 7th edition, John Wiley & Sons (1996).

[20] F. J. Baltá-Calleja, C. G. Vonk, *X-Ray Scattering of Synthetic Polymers*, Elsevier (1989).

[21] L. E. Alexander, *X-ray diffraction Methods in Polymer Science*, John Wiley & Sons, New York (1969).

[22] P. Cebe, B. S. Hsiao, D. J. Lohse, Edts., *Scattering from Polymers*, ACS Symposium Series 739 (1999).

[23] R. Jones, R. A. L. Jones, *Soft Condensed Matter*, Oxford University Press, Oxford (2002).

[24] G. Strobl, *The Physics of Polymers*, Springer, Berlin (1996).

[25] A. Nogales G. Broza, Z. Roslaniec, K. Schulte, I. Šics, B. S. Hsiao, A. Sanz, M. C. García-Gutiérrez, D. R. Rueda, C. Domingo, T. A. Ezquerra, "Low percolation threshold in nanocomposites based on oxidized single wall carbon nanotubes and poly(butylene terephthalate)", *Macromolecules* **37**, 7669-7672 (2004).

[26] D. R. Rueda, M. C. García-Gutiérrez, A. Nogales, M. J. Capitán, T. A. Ezquerra, A. Labrador, E. Fraga, D. Beltrán, J. Juanhuix, J. F. Herranz, J. Bordas, "Versatile wide angle diffraction setup for simultaneous wide and small angle x-ray scattering measurements with synchrotron radiation", *Rev. Sci. Instrum*. **77**, 033904 (2006).

[27] http://smalley.rice.edu/

[28] J. E. Martin, A. J. Hurd, "Scattering from fractals", *J. Appl. Cryst.* **20**, 61-78 (1987).

[29] B. J. Bauer, E. K. Hobbie, M. L. Becker, "Small-angle neutron scattering from labeled single-wall carbon nanotubes", *Macromolecules* **39**, 2637-2642 (2006).

[30] D. W. Schaefer, J. Zhao, J. M. Brown, D. P. Anderson, D. W. Tomlin, "Morphology of dispersed carbon single-walled nanotubes", *Chem. Phys. Lett.* **375**, 369-375 (2003).

[31] W. Zhou, M. F. Islam, H. Wang, D. L. Ho, A. G. Yodh, K. I. Winey, J. E. Fischer, "Small angle neutron scattering from single-wall carbon nanotube suspensions: Evidence for isolated rigid rods and rod networks", *Chem. Phys. Lett.* **384**, 185-189 (2004).

[32] S. Fakirov Edt., *Handbook of Thermoplastic Polyesters-PET, PBT, PEN (Homopolymers, Copolymers, Blends and Composites)*, Wiley-VCH (2001).

[33] E. T. Thostenson, L. Chunyu, T. W. Chou, "Nanocomposites in context", *Compos. Sci. Technol.* **65**, 491-516 (2005).

[34] P. Pöetschke, T. D. Fornes, D. R. Paul, "Rheological behavior of multiwalled carbon nanotube / polycarbonate composites", *Polymer* **43**, 3247-3255 (2002).

[35] L. Zhifei, L. Guohua, F. Wei, Y. Huang, "Microstructure of carbon nanotubes/PET conductive composites fibers and their properties", *Compos. Sci. Technol.* **66**, 1022-1029 (2006).

[36] J. Sandler, M. Shaffer, T. Prasse, W. Bauhofer, K. Schulte, A. H. Windle, "Development of a dispersion process for carbon nanotubes in an epoxy matrix and the resulting electrical properties", *Polymer* **40**, 5967-5971 (1999).

[37] J. M. Brown, D. P. Anderson, R. S. Justice, K. Lafdi, M. Belfor, K. L. Strong, D. W. Schaefer, "Hierarchical morphology of carbon single-walled nanotubes during sonication in an aliphatic diamine", *Polymer* **46**, 10854-10865 (2005).

[38] G. Broza, M. Kwiatkowska, Z. Roslaniec, K. Schulte, "Processing and assessment of poly(butylene terephthalate) nanocomposites reinforced with oxidized single wall carbon nanotubes", *Polymer* **46**, 5860-5867 (2005).

[39] C. Zhao, G. Hu, R. Justice, D. W. Schaefer, S. Zhang, M. Yang, C. Han, "Synthesis and characterization of multi-walled carbon nanotubes reinforced polyamide 6 via in situ polymerization", *Polymer* **46**, 5125-5132 (2005).

[40] K. E. Sichel, Edt., *Carbon Black-Polymer Composites*, Dekker, New York (1982).

[41] M. Connor, S. Roy, T. A. Ezquerra, F. J. Baltá-Calleja, "Broadband ac conductivity of conductor-polymer composites", *Phys. Rev. B* **57**, 2286-2294 (1998).

[42] A. Peterlin, "Drawing and extrusion of semi-crystalline polymers", *Colloid Polym. Sci.* 265, 357-382 (1987).

[43] E. Baer, A. Hiltner, H. D. Keith, "Hierarchical structural in polymeric materials", *Science* **235**, 1015-1022 (1987).

[44] C. Y. Li, L. Li, W. Cai, S. L. Kodjie, K. K. Tenneti, "Nanohybrid shish-kebabs: Periodically functionalized carbon nanotubes", *Adv. Mater.* **17**, 1198-1202 (2005).

[45] S. A. Nitzsche Y. K. Wang, S. L. Hsu, "Application of the molecular simulation technique for clarification of the α↔ βphase transformation in poly(butylene terephthalate)", *Macromolecules* **25**, 2397-2400 (1992).

[46] M .C. García-Gutiérrez, A. Nogales, D. R. Rueda, C. Domingo, J. V. García-Ramos, G. Broza, Z. Roslaniec, K. Schulte, R .J. Davies, T. A. Ezquerra, "Templating of crystallization and shear-induced self- assembly of single-wall carbon nanotubes in a polymer-nanocomposite", *Polymer* **47**, 341-345 (2006).

[47] R. H. Somani, B. S. Hsiao, A. Nogales, S. Srinivas, A. H. Tsou, I. Sics, F. J. Balta-Calleja, T. A. Ezquerra, "Structure development during shear flow-induced crystallization of i-PP: in-situ small-angle X-ray scattering study" *Macromolecules* **33**, 9385-9394 (2000).

[48] G. Kumaraswamy, A. M. Issaian, J. A. Kornfield, "Shear-enhanced crystallization in isotactic polypropylene. 1. Correspondence between in situ rheo-optics and ex situ structure determination", *Macromolecules* **32**, 7537-7547 (1999).

[49] M. C. García Gutiérrez, G. C. Alfonso, C. Riekel, F. Azurri, "Spatially resolved flow-induced crystallization precursors in isotactic polystyrene by simultaneous small- and wide-angle x-ray microdiffraction", *Macromolecules* **37**, 478-485 (2004).

[50] B. Chu, B. S. Hsiao, "Small-angle X-ray scattering of polymers", *Chem. Rev.* **101**, 1721-1761 (2001).

[51] J. M. Samon, J. M. Schultz, B. S. Hsiao, S. Seifert, N. Stribeck, I. Gurke, G. Collins, C. Saw, "Structure development during the melt spinning of polyethylene and poly(vinylidene fluoride) fibers by in situ synchrotron small- and wide-angle X-ray scattering techniques", *Macromolecules* **32**, 8121-8132 (1999).

[52] R. H. Somani, L. Yang, B. S. Hsiao, P. K. Agarwal, H. A. Fruitwala, A. H. Tsou, "Shear-induced precursor structures in isotactic polypropylene melt by in-situ rheo-SAXS and rheo-WAXD studies", *Macromolecules* **35**, 9096-9104 (2002).

[53] M. C. García-Gutiérrez, A. Nogales, D. R. Rueda, C. Domingo, J. V. García-Ramos, G. Broza, Z. Roslaniec, K. Schulte, T.A. Ezquerra, "Microdiffraction and Micro-Raman study on an injection moulding SWCNT-polymer nanocomposite", *Compos. Sci. Technol.* **67**, 798-805 (2007).

1. Introduction

Since the discovery of carbon nanotubes by Iijima in the early nineties [1] the scientific activities in this field have followed an exponential increase due to the remarkable physical properties of this novel form of carbon [1-5]. Carbon nanotubes(CNTs) can be visualized as a graphene layer, essentially a sheet of graphite, which has been rolled up to form a tube (Fig.1).

In particular, some mechanical properties of carbon nanotube have been reported to be outstanding. For example Young Modulus in the range of 1TPa compares with that of diamond (1.2 TPa) while reported tensile strengths (≈200 GPa) are in the range of steel provided CNT density is taken into account [2-4]. Therefore, CNTs are expected to be the basis of a new generation of advanced materials including a new class of polymer nanocomposites [4]. A nanocomposite can be

defined as a nanofilled system in which the total interfacial phase becomes the critical parameter rather than the volume fraction of the filler [4]. The high aspect ratio and nanoscopic dimension of carbon nanotubes provide to CNT-based nanocomposites with specific properties differing from those achieved in classical composites [4-8].

The physical properties of CNTs greatly depend on how sheets have been rolled up, the tube and length diameter, aspect ratio (ratio between diameter and length) and the nanotube morphology. As described in another article of this issue [9], the unique electronic properties of CNT can be assessed by means of Raman spectroscopy which additionally can provide precise information about the tube diameter [10]. Structural information about nanotube morphology can be obtained by means of X-ray scattering [11-13]. X-ray methods can offer structural information at different length scales from the single nanotube to the nanotube bundle. Semicrystalline polymers, composites and in particular SWCNT-polymer nanocomposites are hierarchically organized materials. The understanding of the macroscopic properties in terms of microscopic models requires an analysis of the characteristic order appearing at different length scales. Wide and small angle X-ray scattering techniques provide access to structural information on length scales from inter-atomic distances to about 100 nm. Additionally, in order to fully exploit the nanoscopic functionality of CNTs, and therefore to improve the functionality of the nanocomposite formed by them, a controlled dispersion of the nanotubes within the host matrix is essential [4-17]. Here also X-ray scattering methods may offer crucial information about the level CNT dispersion.

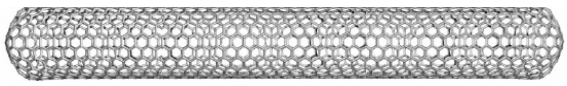

Fig.1. Molecular model of an ideal carbon nanotube.

2. X-ray scattering methods

X-rays were first discovered by Roentgen in 1895 and they were immediately applied to elucidate the inner structure of crystalline solids. It was Max von Laue around 1912 who suggested that crystals behave like three dimensional gratings provoking the phenomenon of diffraction probing that X-rays are electromagnetic waves of very short wave length (≈0.1 nm). X-ray diffraction was fully exploited in 1913 by William Henry Bragg and his son William Lawrence [18]. The basis of X-ray scattering by matter can be found in a great variety of text books where the reader is addressed to look for a deeper understanding of the phenomena [19-22]. X-rays can be obtained from different sources including basically either X-ray generators or synchrotron facilities [20]. In the first case the wavelength depends on the metal used as anode. For copper the characteristic spectral line used is that of wavelength 0.154 nm. For X-ray synchrotron radiation, besides a much higher radiation flux, a tuning of the λ-values is possible. The simplest and probably the most frequently used implication of scattering theory is the Bragg law. By considering crystals as reflection layers for X-rays, W.H. Bragg derived the following equation:

$$d = \frac{n\lambda}{2\sin\theta} \qquad (1)$$

where λ is the wavelength of the X-rays, 2θ is the scattering angle, n is an integral number and d represents the distance between successive identical planes of atoms in the crystal. A visualization of Bragg law is presented in Fig. 2.

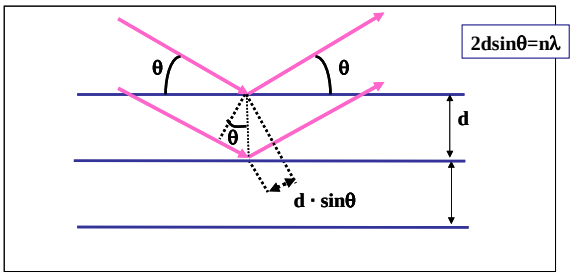

Fig. 2. Scheme to derivate the Bragg law. X-rays (arrows) are reflected by crystallographic planes separated by a distance d.

The different crystallographic planes in a crystal are characterized by the Miller indexes (hkl). These are three integral numbers related to the reciprocal values of the intersection of a given plane with the crystallographic unit cell axes [19]. When the investigated sample is a single crystal then the diffraction pattern consists of a series of spots any of them related to a particular plane in the crystal lattice [19]. However many materials do not appear as single crystals but in a polycrystalline state and therefore the diffraction spots transform into circles due to the different orientation of the crystallites in the sample. An idealized scheme of an X-ray scattering experiment has been shown in Fig.3. When an X-ray beam reaches the sample the diffracted intensity is collected by a suitable detector (photographic film, CCD camera etc). By knowing the experimental conditions (sample to detector distance, size of the detector, wave length of the X-rays) the diffraction pattern can be obtained as a graphic of the diffracted intensity versus either the s-vector (s=2sin(θ)/λ) or the q-vector (q=2πs) or even

versus 2θ. The representation versus the s or q vector is very suitable for two reasons. On one hand, it allows one to represent the scattered intensity as a function of a wavelength independent magnitude. In this way diffraction patterns recorded by using radiation of different wavelength (X-ray, neutrons, light etc) can be easily compared. On the other hand, as derived from the Bragg law, those *s* or *q* values at which a peak in the intensity is observed should correspond to diffracting crystalline planes separated a distance $d=1/s=2\pi/q$.

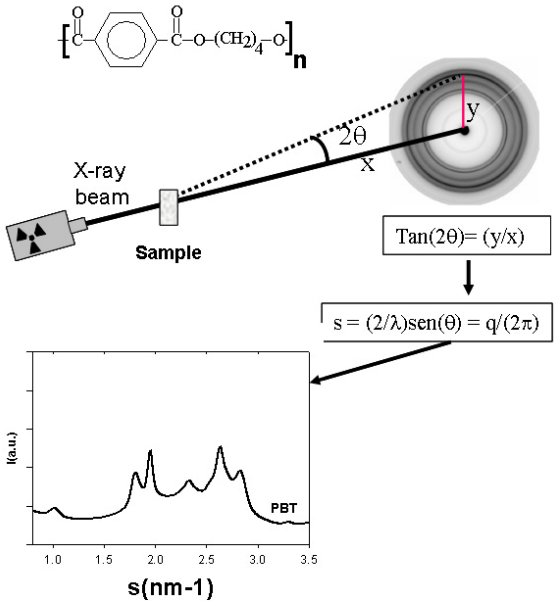

Fig. 3. Scheme of an X-ray diffraction experiment. Knowing the sample to detector distance (x), the wavelength of the X-rays (λ) and the position of a given diffraction ring (y) the scattering angle can be calculated as the arc tan(y/x). The different diffraction maxima following a radius (y-direction) can be represented as plots of the intensity versus the s-vector.

In typical crystalline substances the crystalline planes are separated by distances in the range of 0.1-1 nm. However, soft condensed matter, in general, includes a great variety of complex materials which frequently present a hierarchical structure ranging from tenths to hundreds of nanometers [20-24]. For example, semicrystalline polymers present a characteristic lamellar morphology consisting of stacks of laminar crystals intercalated by amorphous regions [20-24]. The lamellar stacks are characterized by the thickness of the crystals (l_c) and that of the amorphous layers (l_a). Both characteristic lengths define the long period as $L=l_a+l_c$ which is of the order of 10 nm. Depending on the sample to detector distance different length scales can be probed or, in other words, different scattering angles can be accessible. Figure 4 shows a scheme for X-ray scattering experiment in which structural information at different length scales can be obtained.

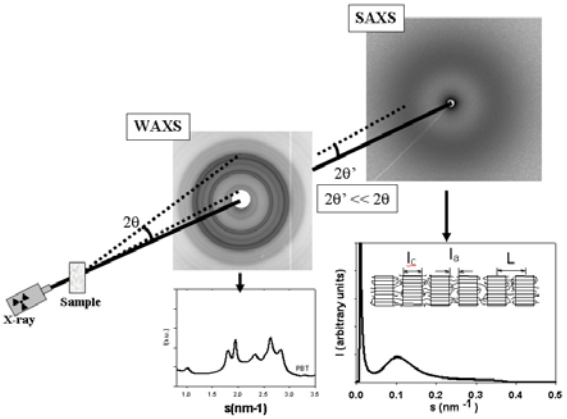

Fig.4. Scheme for X-ray scattering experiment in which structural information at different length scales can be obtained. The first detector leaves a space close to centre to allow the diffracted intensity at lower angles to be detected by a second detector far away from the first one.

For $2\theta > 1^o$ the diffraction experiment is referred to as wide angle X-ray scattering (WAXS). For $1^o > 2\theta > 0.3^o$ one speaks about medium angle X-ray scattering (MAXS) and for $2\theta < 0.3^o$ of small angle (SAXS). The example shown in fig. 4 correspond to a sample of the polymer poly(butylene terephthalate) (PBT) [25]. In the first detector, WAXS-region, the circles correspond to the diffraction of the crystalline phase of PBT. In the second detector, the SAXS-region, the observed broad circle appears as a consequence of the diffraction of the consecutive laminar crystals separated by amorphous layers (a scheme of this morphology is shown in the inset of the SAXS intensity profile). Both, WAXS and SAXS have been shown to be of great importance while dealing with the structural analysis of soft condensed matter because structural characterization of different building blocks of a complex material can be obtained [20-26].

3. Morphology of carbon nanotubes

3.1. The single carbon nanotube

Carbon nanotubes adopt basically two characteristic morphologies, either possessing a single wall or having multiple walls. In the first case one speaks about single wall carbon nanotubes (SWCNTs) while in the second case one refers to multi wall carbon nanotubes (MWCNTs). SWCNTs are made from a single graphene layer, which is a hexagonal carbon network, where the way in which the layer is rolled up determines the chirality of the nanotube and controls the electronic properties [9,10]. MWCNTs consist on concentric single walled tubes, where each individual tube may have different chirality. The mechanical stability of MWCNT is

provided by Van der Waals forces which held together the concentric nanotubes. Figure 5(a) shows a high resolution transmission electron micrograph (TEM) of a SWCNT [14] which, as reported by M. Terrones [5], is probably the first image of a SWCNT ever taken. The SWCNT consists of an individual graphene cylinder with a diameter of about 4 nm. Due to the fact that in an isolated SWCNT only one graphitic layer is involved X-ray diffraction is absent because, as mentioned in the previous paragraph, the diffraction condition requires the existence of several planes repeating periodically in real space. Figure 5(b) shows a TEM image of a MWCNT where one visualizes several layers of graphitic carbon rolled leaving a hollow space in the centre [15]. Contrary to the SWCNT case, the presence in an isolated MWCNT of several graphitic layers fulfils the diffraction condition and therefore characteristic diffraction patterns are available.

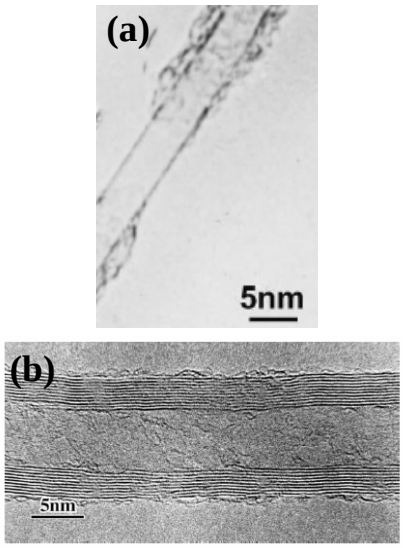

Fig. 5. (a) High resolution transmission electron micrograph (TEM) of a SWCNT reproduced from Ref. [5]. (b) TEM image of a MWCNT, several layers of graphitic carbon leaving a hollow space in the centre are visible. Reproduced from [5] and [15] with permission.

Figure 6 shows one of these patterns for a MWCNT from Nanocyl S.A. Figure 6(a) shows the two dimensional diffraction pattern with a characteristic ring. The radial intensity profile of this pattern (see Fig. 3 for procedure) reveals the presence of the peak corresponding to the ring appearing at q = 18 nm^{-1} characteristic of the 002 reflection from the graphite layer structure. This value leads to a spacing value of $d=2\pi/q_{max}=0.35$ nm for the distance between the graphitic layers. This value is in agreement with those found for standard graphite. Accordingly, X-ray diffraction may provide information about the nature, either SWCNT or MWCNT, of carbon nanotubes.

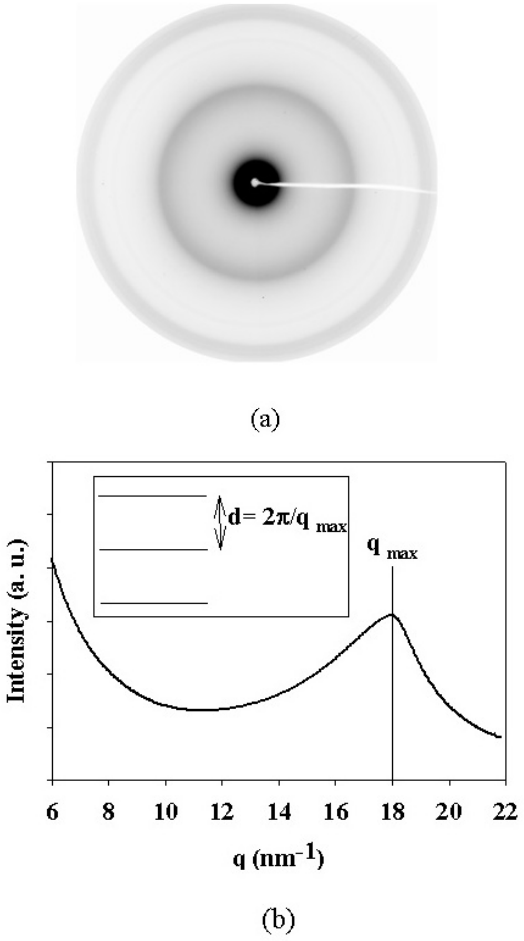

Fig. 6. (a) X-ray pattern for a MWCNT. (b) Radial intensity profile of the pattern in one dimension revealing the presence of the 002 reflection of the graphite layer structure.

Both SWCNT or MWCNT can be produced by a great variety of techniques including arc-discharge, laser ablation, gas-phase catalytic growth from carbon monoxide and chemical vapour deposition from hydrocarbons [5,15]. Seeking for realistic industrial or technological applications, large quantities of nanotubes are required. During the synthesis of carbon nanotubes several impurities appear including catalyst particles, amorphous carbon and non-tubular graphitic entities. Therefore, depending on the application, a subsequent purification treatment is sometimes required. In principle, gas-phase procedures are reported to produce less impurities and therefore are very appropriate to scale-up nanotube production [15]. Nowadays there are several companies providing carbon nanotubes on an industrial basis. For example, Carbon Nanotechnologies Inc.(CNI) Houston TX, USA, involved in the large-scale production of high-purity SWCNTs, uses a technology based on the developments of Richard E.

Smalley who was awarded the 1996 Nobel Prize in Chemistry for his co-discovery of Buckyballs. Here a gas-procedure, namely the high-pressure conversion of carbon monoxide (HiPco) [16] is used to obtain significant amounts of SWCNT. Another example of academia-industry successful partnership is provided by the English company Thomas Swan&Co which is manufacturing SWCNT on the basis of a chemical vapour deposition (CVD) method developed at the University of Cambridge, UK [17].

3.2 The bundle of carbon nanotubes

As a consequence of the preparation conditions or due to chemical affinity carbon nanotubes never are obtained as isolated tubes. A typical carbon nanotube sample consists of micron-size aggregates, frequently referred to as bundles, in which from some tens to some hundreds of single nanotubes self-assemble in a two-dimensional hexagonal lattice held together by van der Waals interaction [11-13]. Fig. 7 presents a TEM image of a characteristic bundle of SWCNTs [27]. The diffraction of such a hexagonal lattice of carbon nanotubes appears mainly due to the characteristic (1 0) planes schematized in Fig. 7. Figure 8 shows the 2D X-ray scattering pattern of a SWCNT sample (purified HiPco from CNI) and the diffractogram obtained from the radial integration of the 2D pattern (see procedure in Fig. 3). The 2D X-ray scattering pattern indicates a highly pure SWCNT, as there is not any signal from the 002 reflection of the graphite as usual contaminant.

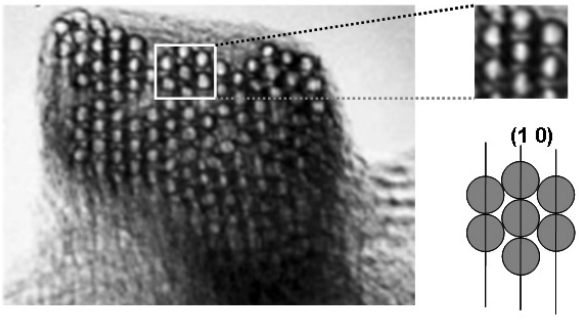

Fig. 7. TEM image of a characteristic bundle of SWCNTs [27]. Each SWCNT may have a diameter of 1.5nm. Enlargement shows the hexagonal crystal lattice characteristic of carbon nanotube bundles. Scheme show the characteristic planes of the two dimensional hexagonal lattice.

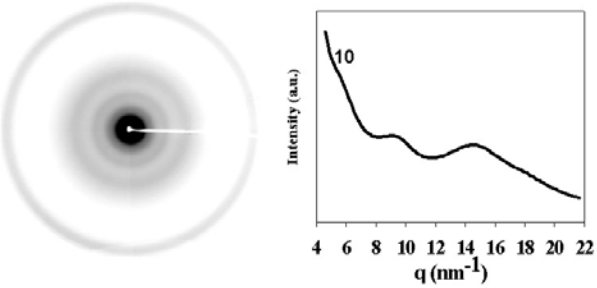

Fig. 8. 2D X-ray scattering pattern of a SWCNT sample (purified HiPco from CNI) and the diffractogram obtained from the radial integration of the 2D pattern.

The diffractogram exhibits a shoulder at $q \approx 4.4$ nm^{-1} corresponding to the characteristic (1 0) reflection of a closely-packed two-dimensional hexagonal lattice and several maxima at higher q-values corresponding to other reflections from the hexagonal packing. However, the peaks are broad as fluctuations of the lattice constant induced by tube diameter polydispersity are expected. The (1 0) peak in the raw data is affected by a strong continuous scattering due to the contribution of nanoparticles of different carbonaceous species and of nanovoids. As easily deduced from Fig. 7, the spacing value d=1/q is closely related to the tube diameter.

3.3 The aggregate of bundles of nanotubes

The bundle of single carbon nanotubes is not the final morphological step of a nanotube sample. Due to the preparation procedure most of the carbon nanotube synthesis methods lead to a final product consisting of micron-size aggregates of nanotube bundles. Figure 9 shows a scanning electron microscopy (SEM) picture to illustrate these aggregates for a sample of SWCNTs (HiPco from CNI).

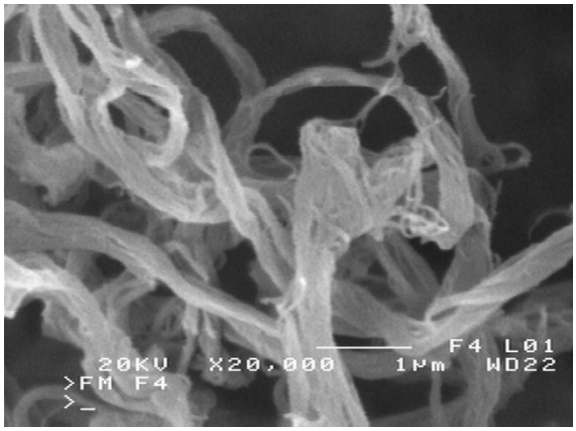

Fig. 9. Scanning electron microscopy (SEM) showing micron-size aggregates of SWCNTs (HiPco from CNI).

The morphology consists of highly branched aggregates constituted by relatively thick ropes filling the space in a disorder manner. This type of aggregates can be described as being fractal objects [28]. A fractal can be defined as a self-similar object over a range of sizes. For example, if a fractal structure is viewed at different magnifications the structure should be the same. An example for that could be a long and thin rod. For magnifications smaller than its length the rod appears as a straight line of infinite length. Only when the magnification reaches the diameter dimensions the structure starts to look different. Scattering from fractals of different nature, from carbon-black to polymers in solution, has been described extensively in the literature [28-31]. Scattering experiments in fractals, either with light, neutrons or X-rays have shown that the scattering intensity follows a power law as $I(q) \propto q^{-\alpha}$. Due to the size of the scattering objects, much bigger than the crystal spacings probed by wide angle techniques (WAXS), scattering in this case requires its small-angle(SAXS) version (Fig. 4). Values of α=1,2,3 are expected when the scattering objects are rods, discs and spheres respectively [28]. Intermediate cases $2<\alpha<3$ are characteristic of objects possessing a fractal geometry [28-31]. Accordingly, if one had individual carbon nanotubes, or individual rod-like bundles, then a scattering experiment should provide an exponent α=1 as schematized in Fig. 10(a). Recently small-angle scattering measurements, both with neutrons or with X-rays, have been reported on SWCNT dispersed in liquids [29-31]. Values of $\alpha \approx 2$-2.5 were found indicating two basic features: (a) SWCNT aggregates form structures of fractal nature, and (b) the dispersion of carbon nanotubes down to the elemental level of a single nanotube is a quite complex task. As an example, Fig. 10(b) shows the SAXS intensity as a function of the q-vector for a dispersion of SWCNT (HiPco) in a molten polymer, namely poly(ethylene terephthalate)(PET), at T=290^{o}C well above its melting temperature [32].

The results are plotted in a double logarithmic scale to emphasize the power law behaviour. An initial value of 2.7 for the polymer matrix suddenly decreases for concentrations of SWCNTs higher than about 0.1 % and then levels off towards a limiting value of ≈2.1. Similarly to what it has been reported for dispersion of SWCNTs in liquids [29-31] the results of fig.10b indicate the absence of the clear signature of individual rod-like scatters which would produce slope values of α=1. On the contrary the observed slopes in the region of 2.1 for the dispersion of SWCNT within the polymer molten matrix can be interpreted as due to the scattering of a mass fractal consisting of SWCNT agglomerates. To be precise experiments shown in fig. 10b are done for a polymer-carbon nanotube composite. However, due to the fact that the polymeric matrix is in its molten state the peculiarities of these types of composites do not arise as they do as the polymeric matrix solidifies. We will see this in the next paragraph.

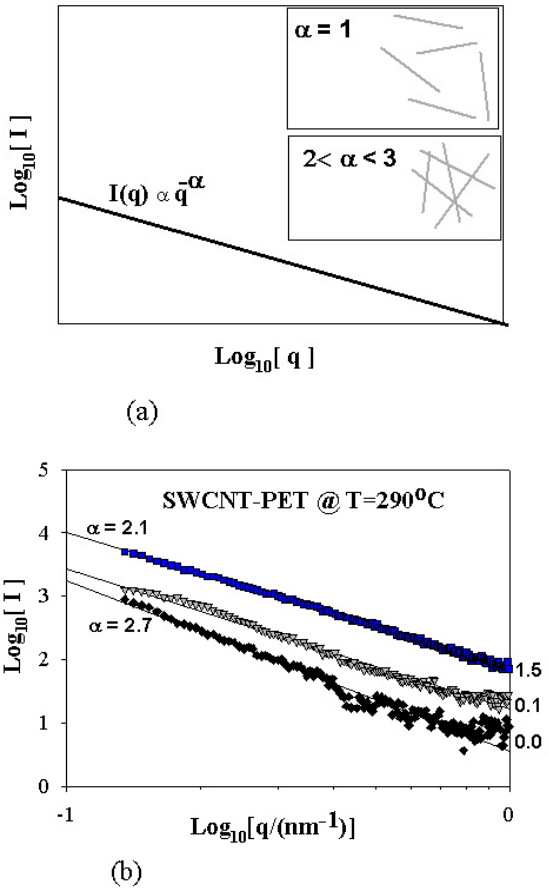

Fig. 10. (a) The scattered intensity by a fractal follows a potential law on q. Exponents α=1 are expected when the scatterers are individual rods. Exponents $2<\alpha<3$ are expected for rod aggregates. (b) Scattered intensity as a function of the q-vector plotted in a double logarithmic scale for SWCNT dispersed in molten PET. SWCNT weight % concentration labelled on the right.

4. Morphology of polymer-CNT nanocomposites

4.1 Dispersion of CNTs within the polymer matrix

Due to their extraordinary mechanical properties like an extremely high Young's modulus, stiffness and flexibility [15,33], SWCNTs are ideal structural reinforcements for polymer nanocomposites. In order to transfer the outstanding properties of SWCNT to the composite material from the nano to

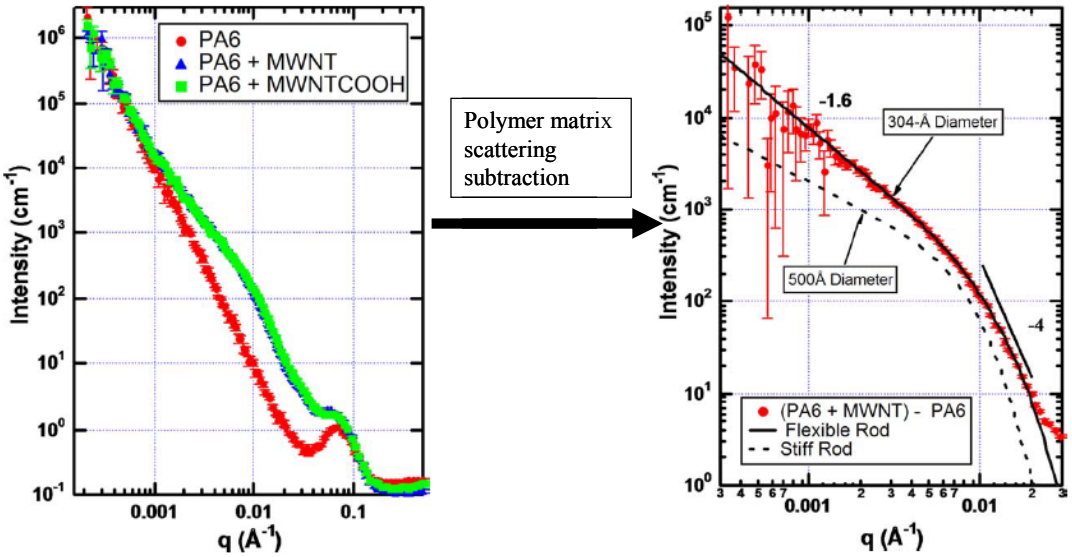

Fig.11. (Left) X-ray Scattered intensity as a function of q in double logarithmic scale for a polyamide6 (PA6) and PA6-MWCNT nanocomposite at room temperature. (Right) Data after subtraction of the scattering from the PA6 matrix. The continuous and dashed lines are the expectation of different models considering different nanotube diameters. Data taken from Ref. [39] with permission from Elsevier.

microscale, essential steps involve dispersion of the SWCNT within the polymer matrix and processing of the nanocomposite. Dispersion of carbon nanotubes in polymers has been attempted by a great variety of methods [15,33] from mixtures with thermoplastics [34,35] or with curing epoxies [36,37] to in situ polymerization of monomers in the presence of CNTs [38,39] among many others. A common feature up to now is the absence of an optimal dispersion of single carbon nanotubes as revealed by SAXS measurements. As an example Fig 11 shows the SAXS scattered intensity for a composite made of MWCNTs and Polyamide 6 [39]. The scattering data exhibit a strong maximum around q=0.07 nm^{-1} related to the long spacing of the polymer matrix. After subtraction of the scattering from the polymer matrix (Fig. 11 right) scattering data display two linear regions both with slopes $\alpha > 1$. As mentioned in section 3.3, the absence of a q-region with slopes close to 1 is an indicative of nanotube aggregation. The absence of a perfect dispersion can have strong impact in the mechanical properties of the nanocomposite. The presence of a fractal rope network may provoke a weakening of the mechanical properties because of significant deformation by bending [30]. However, as far as the electrical properties are concerned, the situation could be quite the opposite. It is known for long time, in the field of carbon-black polymer composites, that the level of aggregation favours the formation of a conducting network by decreasing the percolation threshold [40,41].

4.2 Morphology induced by processing

As far as processing is concerned, different methods have been described [33]. If the polymer matrix is a semicrystalline polymer then injection moulding is a very appropriate method to produce items [38] like those shown in Fig. 12. These pieces correspond to a PET-SWCNT nanocomposite injection moulded with a Baby Plast, Model 6/10 (Cronoplast S.L. Comp) injection moulding machine into long pieces with a rectangular cross section of 2x4 mm^2. The injection moulding parameters were: injection pressure 25 bar, melt temperature 240-250 ºC, mould temperature 40 ^{0}C, holding time 6 s and cooling time 20 s. In this case the sample shape is appropriate for mechanical testing.

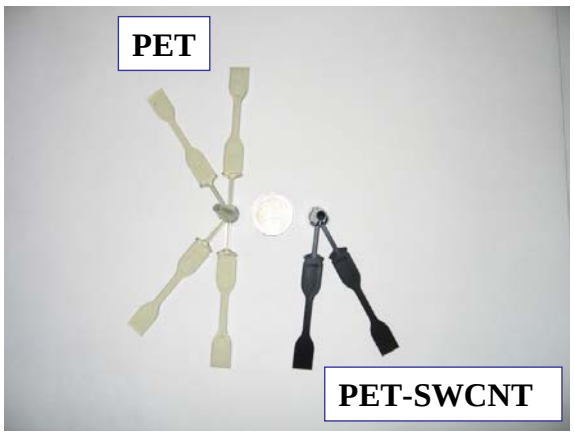

Fig. 12. Injection moulded pieces from PET and PET-SWCNT (0.2 weight % of SWCNT) prepared for mechanical testing. In the centre a 2€ coin for size evaluation is shown.

A SEM image of a cryogenic fracture for a PET-SWCNT nanocomposite with 0.3 weight % of SWCNT is shown in Fig. 13. The bundles and aggregates of carbon nanotubes appear as the bright elements.

By imposing flow fields to a crystallizing polymer melt the rate of crystallization can be accelerated and also the formation of oriented morphologies can be induced [42]. Semicrystalline polymers, composites and in particular SWCNT-polymer nanocomposites can be considered as hierarchically organized materials [24,43,44]. The understanding of the macroscopic properties in terms of microscopic models requires an analysis of the characteristic order appearing at different length scales. Therefore WAXS and SAXS techniques can provide structural information on different length scales. Figure 14(a) presents a scheme of a PBT-SWCNT injection moulded sample [46]. The maximum uniformity of the flow fields is achieved in the central part of the piece. Both WAXS and SAXS patterns for pure PBT, recorded with the beam perpendicular to the flow direction, are shown in Fig. 14(b). The patterns exhibit characteristic features of semicrystalline PBT. The observed reflections from WAXS correspond to the α crystalline phase [45]. The broad ring in the SAXS region corresponds to the long period which indicates the existence of an isotropic alternation of crystalline lamellae and amorphous layers, related to the nanostructure typical of semicrystalline polymers (fig14d). Fig.14c shows the X-ray scattering pattern from the PBT-SWCNT nanocomposite with 0.2 weight % of nanotubes. In the WAXS pattern, additionally to the structural features of the PBT matrix, there appears an additional ring (signalled by an arrow and enlarged as an inset). This additional reflection present in the WAXS pattern of the nanocomposite is position dependent being detectable at positions starting from the edge of the sample until about 1 mm towards the centre of the sample [46]. The extra reflection corresponds to a non-hexagonal ordered assembling of SWCNT. Considering that this unexpected packing of SWCNT appears in the regions close to the walls of the sample it seems plausible to attribute it to the shear stress which reaches a maximum in these regions and tends to zero in the centre of the sample [46] On the other hand SAXS patterns reveal a clear orientation characterized by a concentration of the scattered intensity on the meridian and a equatorial streak. The orientation is not position dependent as identical SAXS patterns were recorded when the sample is rotated 90º.

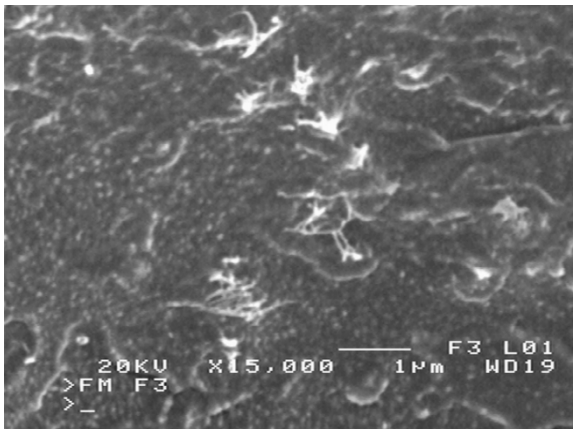

Fig. 13. SEM image of an injection moulded pieces of PET-SWCNT with (0.3 weight % of SWCNT. Bright filaments and aggregates is the carbon nanotube additive.

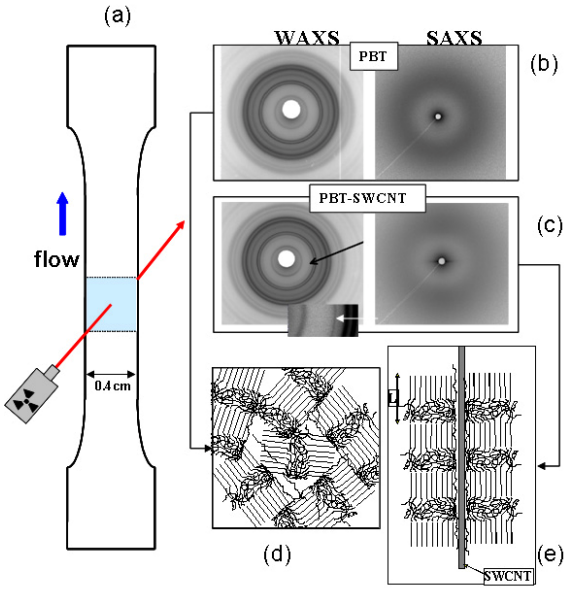

Fig. 14. (a) Scheme of a PBT-SWCNT injection moulded sample [46]. (b) WAXS and SAXS patterns for pure PBT and (c) for PBT-SWCNT nanocomposite, with 0.2 weight % of carbon nanotubes, recorded with the beam perpendicular to the flow direction. The inset in the WAXS of PBT-SWCNT is an enlargement of the region indicated by the arrow to highlight the appearance of a new reflection. (d) Scheme of an isotropic alternation of crystalline lamellae and amorphous layers, related to the isotropic X-ray patterns for PBT. (e) Model of a hybrid shish-kebab structure, where the SWCNT act mainly as the shish and the epitaxially growth polymer crystals perpendicular to the SWCNT are the kebabs.

It is well established that flow fields on a crystallizing polymer melt can accelerate the rate of crystallization and induce the formation of oriented morphologies [47-49]. The stability, after flow cessation, of the oriented morphology is a compromise between crystallization and chain relaxation [49]. Processing operations of commercial

polymer such as extrusion, injection moulding, film blowing or fibre spinning, subject a polymer melt to intense flow fields (shear, elongational or mixed) and crystallization occurs from a distorted melt [50]. In the case of PBT the flow conditions are not enough to produce oriented morphology as derived from the SAXS patterns revealing isotropic rings. However for the nanocomposite, the existence of oriented crystallization morphology is evident as revealed by the anisotropic SAXS signals. The equatorial intensity can be interpreted as due to bundles of parallel chain segments preferentially oriented along the flow direction following the orientation of SWCNT in this direction (shish structures), while the meridian maximum observed is consistent with the presence of layered lamellar assemblies (kebab) growing epitaxially from the shish structures in a direction perpendicular to their axis [51,52]. This situation could be represented by a model of a hybrid shish-kebab structure (Fig. 14(e)), where the SWCNT act mainly as the shish and the epitaxially growth polymer crystals perpendicular to the SWCNT are the kebabs [53]. The obtainment of oriented polymer crystals is a technological goal because significant improvement of important mechanical properties such as the Young modulus can be achieved. In the case of PBT-SWCNT an increment of about a 18 % in the Young modulus from 2.24 GPa for PBT to 2.65 GPa for the 0.2 % nancomposite has been measured from extension strain-stress experiments [38,46].

5. Conclusion

We have shown that wide and small angle X-ray scattering techniques (WAXS and SAXS respectively) can be a valuable tool to characterize the structure of carbon nanotubes(CNT) and related CNT-polymer nanocomposites at the different characteristic length scales. From lower to higher dimensions, the hierarchy of structures includes single CNTs, bundles of CNTs and aggregates of CNT bundles. Additionaly, when CNTs are added to a polymer matrix to form a nanocomposite, X-ray scattering may offer information about CNT dispersivity and about the effect of nanocomposite processing. The structural information obtained by means of X-ray scattering can be crucial in order to design new materials based on carbon nanotubes.

Acknowledgements

The authors thank the financial support from the MCYT (grant MAT2005-01768), Spain. The help of G. Broza, Z. Roslaniec, K. Schulte, I. Sics, B. H. Hsiao, S. S. Funari in different parts of this work is gratefully acknowledge. M. C. G.-G. and A. N. are also grateful to the Ramón y Cajal Program for the support of this reserach

